Phase Transition from Disordered Sphere to Hex-Cylinder via Transient Ordering into Bcc-Sphere in SIS Triblock Copolymer†

Norihiro Sota, Naoki Sakamoto,‡ Kenji Saijo, and Takeji Hashimoto*

Department of Polymer Chemistry, Graduate School of Engineering, Kyoto University, Kyoto 606-8501, Japan

Received March 6, 2003; Revised Manuscript Received April 18, 2003

ABSTRACT: We have investigated the ordering processes from the disordered-sphere phase (designated hereafter disordered sphere), where spherical microdomains exist but they have only a short-range liquidlike order, to the phase of hexagonally packed cylindrical microdomains (designated hereafter hex-cylinder), induced by the temperature drop (*T*-drop). The block copolymer studied is a compositionally asymmetric polystyrene-*block*-polyisoprene-*block*-polystyrene triblock copolymer and forms disordered sphere above the order−disorder transition temperature involving the lattice disordering−ordering transition temperature, T_{ODT} or T_{LDOT}, spheres in a body-centered-cubic lattice (designated hereafter bcc-sphere) below T_{LDOT} but above the order−order transition (OOT) temperature, T_{OOT}, and hex-cylinder below T_{OOT}. The ordering processes induced by *T*-drop were explored in situ and at a real time by using time-resolved small-angle X-ray scattering, and the transient microdomain structures developed during the ordering processes were observed by a transmission electron microscope and a polarized optical microscope for specimens rapidly frozen below the glass transition temperature at particular times in the ordering processes. We confirmed that the freeze-in process does not change the long-range order of the system. When the specimen is deeply quenched into the temperature range below T_{OOT}, hex-cylinder is directly formed from disordered sphere. However, when the specimen is shallowly quenched below T_{OOT}, bcc-sphere is first formed from disordered sphere and fills the whole sample space. Then bcc-sphere is transformed into hex-cylinder. This striking ordering process first involves the ordering into a metastable structure followed by the OOT into a stable structure.

I. Introduction

Block copolymers exhibit various phase transitions. One typical transition is the microphase-separation transition or the order−disorder transition (ODT),[1−4] which is the transition between a phase composed of microdomains having a long-range order and a disordered phase. Compositionally symmetric or nearly symmetric block copolymers having lamellar or hexagonally packed cylindrical microdomains (hereafter denoted as hex-cylinder) with long-range order transform directly into the disordered state, where constituent block chains are mixed on a molecular basis with only thermally induced composition fluctuations, on the heating process.[5−11] However, highly asymmetric block copolymers having spherical microdomains in a body-centered-cubic lattice (hereafter denoted as bcc-sphere) first transform into spheres or micelles with a short-range liquidlike order, which are referred to as "disordered sphere", followed by a transformation into the disordered state free from spheres (or micelles) as temperature increases.[12−19] The phase transition between bcc-sphere and disordered sphere is referred to as the lattice disordering/ordering transition (LDOT) or ODT involving the LDOT process.[17−19] The order−order transition (OOT) from one type of ordered microdomain structure to another is also known as another phase transition in block copolymers. In the strong segregation limit, the morphology basically depends only on the volume fraction of one of constituent block chains, *f*,[4,20−22] while in the weak segregation regime, it depends not only on *f* but also on χN,[1,2,4,23−25] where χ and N are the Flory's segmental interaction parameter and total degree of polymerization, respectively. Therefore, the OOT between different kinds of microdomain structures can occur by changing temperature in this regime.[16,26−46] For example, some works have been reported on OOT between lamella and hex-cylinder,[28−30,46] OOT between hex-cylinder and bcc-sphere,[16,31−37] OOT between lamella and gyroid,[38−41,46] and OOT between gyroid and hex-cylinder.[42−46]

It is very important to explore and clarify the processes and dynamics of the phase transitions from a viewpoint of understanding their molecular assemblies and physical properties. So far, the ordering dynamics have been studied by using various methods such as small-angle X-ray scattering (SAXS),[47−55] small-angle neutron scattering,[56] rheology,[57−59] and depolarized light scattering.[60−62] Moreover, the real-space observations on the ordering processes were conducted by using transmission electron microscopy (TEM) as described below.

The ordering processes of the lamellar microdomains induced by a temperature drop (*T*-drop) from the disordered state were explored in situ as a function of time by using time-resolved SAXS.[52,54,63,64] Furthermore, the structures during the ordering processes were observed under TEM on the specimens frozen at various times in the ordering processes.[63,64] It was revealed that the ordering at shallow quenches proceeded via the nucleation and growth process: Even after the quench into the ordered state, the system remains in the

† Presented in part in Photon Factory Activity Report 1998, #16, Part B; High Energy Accelerator Research Organization (KEK); p 122, and in Polymer Preprints, Japan, 1999; The Society of Polymer Science, Japan; Vol. 48, No. 11, p 2814.

‡ Present address: Computer Science Department, Asahi Chemical Industry Co., Ltd., 2-1, Samejima, Fuji, Shizuoka 416-8501, Japan.

* To whom correspondense should be addressed: e-mail hashimoto@alloy.polym.kyoto-u.ac.jp.

10.1021/ma034291i CCC: $25.00
Published on Web 05/23/2003

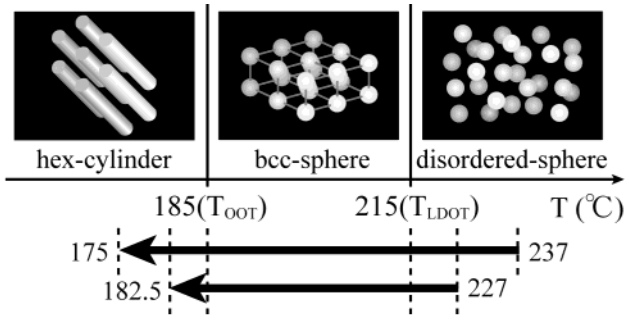

Figure 1. Schematic illustration of the phase behavior for the SIS triblock copolymer and of the temperature-drop experiments from the disordered-sphere phase to the hex-cylinder phase.

disordered state for a certain incubation period. After this incubation period, the lamellar grains are nucleated in the disordered state and grow at the expense of the disordered phase, and finally the system is volume-filled with the ordered grains. Moreover, the lamellar grains coexisting with the disordered matrix were elucidated to have essentially a prolate ellipsoidal shape with a larger size along lamellar normal than directions perpendicular to it.[64]

The ordering processes from disordered sphere to hex-cylinder and from disordered sphere to bcc-sphere have also been studied for an asymmetric polystyrene-*block*-polyisoprene-*block*-polystyrene (SIS) triblock copolymer.[65] This triblock copolymer forms hex-cylinder below the OOT temperature (T_{OOT}) of 185 °C and bcc-sphere above it. The bcc lattice is distorted above the LDOT temperature (T_{LDOT}) of 215 °C and transformed into disordered sphere. Disordered sphere was reported to be stable up to 237 °C, the highest experimental temperature employed (see Figure 1). The ordering processes described above were also investigated by *T*-drop methods and explored by time-resolved SAXS and by TEM on frozen samples. It was revealed that the orderings after the *T*-drop proceeded via the nucleation and growth process. The system stays at the disordered-sphere state for a certain incubation period. After this incubation period, hex-cylinder or bcc-sphere appears and grows at the expense of the disordered-sphere phase. The shape of the ordered grains of hex-cylinder was a lenslike oblate ellipsoid in which the cylinders were oriented with their axes parallel to the revolution axis, while that of bcc-sphere was nearly spherical.

We should note here that effects of the quench depth from T_{OOT} on the ordering processes of hex-cylinder were not explored for the asymmetric SIS triblock copolymer reported above. It is expected that the ordering processes depend on the quench depth from T_{OOT}. Therefore, in this study, we aim to investigate whether there is a difference in the ordering processes of hex-cylinder between a deep quench and a shallow quench. In particular, we focused our interest on whether or not the system brought in the shallow quench will form transiently a bcc-sphere during the ordering into hex-cylinder.

II. Experimental Method

The sample used in this study is a SIS triblock copolymer (Vector4111, Dexco Polymers Co.). The weight-averaged molecular weight, M_w, is 1.4×10^5, and the polydispersity index, M_w/M_n, is 1.11 with M_n being the number-averaged molecular weight. The weight fraction of PS is 0.183. The details of the sample's characterization were presented elsewhere.[16,65] The sample was dissolved in toluene with a small amount of antioxidant (Irganox 1010, Ciba-Geigy Group) to prepare a 10 wt % solution, and then the solvent was evaporated slowly in a fume hood for 1 week and annealed at 170 °C in a vacuum oven for a half day.

T_{OOT} and T_{LDOT} of the SIS triblock copolymer were determined to be 185 and 215 °C, respectively, with the static SAXS experiments.[65] The phase behaviors of the SIS triblock copolymer thus obtained are schematically illustrated in Figure 1.

The orderings of hex-cylinder from disordered sphere were explored by the *T*-drop experiments. In one experiment, the specimen was deeply quenched at a temperature, T_{cyl}, below T_{OOT} from 237 to 175 °C; i.e., the quench depth from T_{OOT}, ΔT ($\equiv T_{OOT} - T_{cyl}$), is 10 °C, and the thermodynamic driving force, ϵ, defined as ϵ ($\equiv \Delta T/T_{OOT}$), is 0.0540. In another one, the specimen was shallowly quenched below T_{OOT} from 227 to 182.5 °C; i.e., ΔT is 2.5 °C and ϵ is 0.0135. We adopted the same quenching method as that in ref 65, and the ordering processes after *T*-drop were observed with time-resolved SAXS. First, the specimen placed in the sample holder[66] was put in a heater block which was set on the optical path of the incident X-ray beam and regulated at the initial temperature above the T_{LDOT}, 227 or 237 °C for 10 min, and then the temperature of the heater block was rapidly changed into T_{cyl}. The time-resolved SAXS experiments were started, and the starting time was set zero when the sample temperature reached the measuring temperature, T_{cyl}. The specimen reached the measuring temperature in ca. 2 min after *T*-drop. Note that 2 min delay is not practically important at all, because the delay time is much shorter than the incubation time as will be clarified later.

The SAXS apparatus used was described in detail elsewhere.[67−69] It consists of an 18 kW rotating-anode X-ray generator (SRAM18XH MAC Science Co. Ltd.) with a graphite crystal monochromator to obtain Cu Kα beam with a wavelength of 0.154 nm, a vacuum chamber for the incident-beam path and scattered beam path, and one-dimensional position-sensitive proportional counter (PSPC) with line focus optics.

The SAXS profiles were measured with the generator power of 12 kW (40 kV and 300 mA) and with varying exposure time to incident X-ray beam in the range of 60−3000 s and corrected for the absorption of the sample, air scattering, background scattering arising from thermal diffuse scattering (TDS),[72] and slit-height and slit-width smearing,[67−69] unless otherwise stated. The absolute SAXS intensity was obtained by using the nickel-foil method.[71] The intensity level of TDS was assumed to be a constant and was determined from the slope of Iq^4 vs q^4 plot at the high-q region ($q > 0.7-1.1$ nm^{-1}).[72]

TEM and POM observations of the structures during the orderings were also conducted. For this purpose, the specimens during the orderings at given times after *T*-drop to T_{cyl} were quenched into the ice−water (at 0 °C) to freeze ordering structures by using the same method as that used in the previous works.[63−65] The structures can be frozen because the glass transition temperature, T_g, of the matrix PS phase (ca. 100 °C) in the block copolymer is higher than 0 °C. For the preparation of TEM observations, the frozen specimens at 0 °C were microtomed into the ultrathin sections of ca. 50 nm thickness at −100 °C with a Reichert-Jung ultracut E together with a cryogenic unit FC 4E and a diamond knife (DiATOME, Switzerland). The ultrathin sections were picked up on 400 mesh copper grids and stained by the vapor of 2% O_5O_4(aq) for 1 h at room temperature which was still below the T_g. The staining is known to cross-link PI blocks and to fix PI domains.[73,74] The TEM observations were carried out with a JEOL JEM-2000FXZ transmission electron microscope operated at 120 kV. For the preparation of the POM observations, the frozen specimens were cut into the thin sections of less than 0.2 mm thickness. The POM observations were carried out with a polarized-light optical microscopy (OPTIPHOT-POL, Nikon Corp., Tokyo, Japan) equipped with a CCD camera (XC-711, Sony Corp., Tokyo, Japan) for a detector at room temperature.

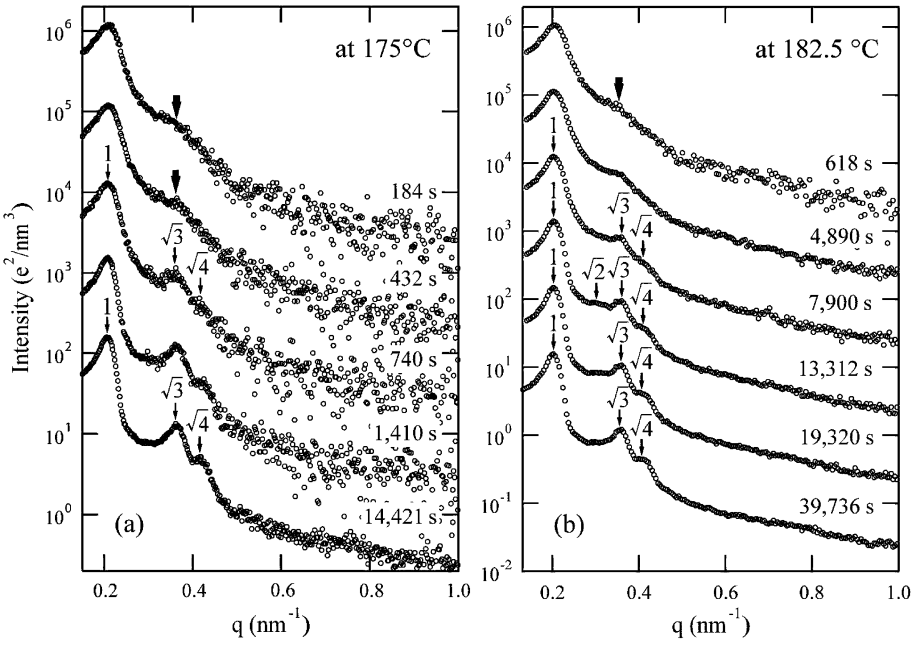

Figure 2. Time evolution of the SAXS profiles for the SIS triblock copolymer after *T*-drop (a) from 237 to 175 °C and (b) from 227 to 182.5 °C at which the equilibrium microdomain structure is hex-cylinder (see Figure 1). The profiles without slit corrections are deliberately shown here to prevent any artifacts that might be induced by the slit corrections.

III. Experimental Results

III.1. SAXS Obsevations. (1) Time Evolution of the SAXS Data. Figure 2 shows the time evolution of the SAXS profiles after *T*-drop (a) from 237 to 175 °C (deep quench) and (b) from 227 to 182.5 °C (shallow quench) plotted as a function of the scattering vector q, defined by $q = (4\pi/\lambda)\sin(\theta/2)$ with λ and θ being the wavelength of the incident X-ray and the scattering angle, respectively. The intensities of the profile shown at the top of this figure are actual values, and the intensities of other profiles are shifted down by one decade relative to the intensities immediately above in order to avoid overlaps. We deliberately show the profiles without silt corrections to prevent any artifacts that might be induced by the corrections and without the TDS correction. Figure 2a previously reported[65] is shown for comparison of the new profiles of Figure 2b in this paper.

The following features can be briefly noted in Figure 2a. The profiles obtained at 184 and 432 s have a broad second-order shoulder at $q = 0.35$ nm^{-1}, marked by a thick arrow. And then higher-order peaks appear at $q = \sqrt{3}q_m$ and $\sqrt{4}q_m$, where q_m is the wave vector at the first-order peak, and are getting sharper as time goes by after 740 s. On the other hand, the following features can be noted for new data set shown in Figure 2b. The profile obtained at 618 s have a second-order shoulder at $q = 0.35$ nm^{-1}, marked by a thick arrow. In the profiles obtained at 4890 and 7900 s, higher-order peaks appear at $q = \sqrt{3}q_m$ and $\sqrt{4}q_m$ and are getting sharper as time goes by. Then, in the profile obtained at 13 312 s, higher-order peaks can be clearly seen at $q = \sqrt{2}q_m$, $\sqrt{3}q_m$, and $\sqrt{4}q_m$. The higher-order peak at $q = \sqrt{2}q_m$ disappears, and the higher-order peaks at $q = \sqrt{3}q_m$ and $\sqrt{4}q_m$ are getting sharper as time goes by after 19 320 s. Finally, the higher-order peaks can be seen only at $q = \sqrt{3}q_m$ and $\sqrt{4}q_m$. Comparing these two figures, it is found that there is a difference in the time evolution of the SAXS profiles between the two *T*-drop experiments.

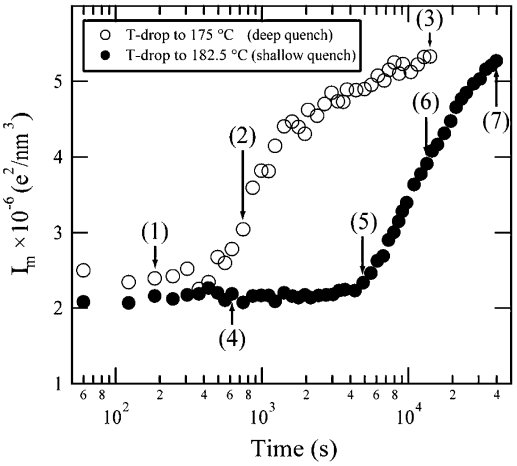

Figure 3. Time evolution of the maximum intensity for the desmeared SAXS profile I_m for the SIS triblock copolymer after *T*-drop from 237 to 175 °C and from 227 to 182.5 °C. The specimens are frozen for TEM observations at the time shown by the arrows numbered (2) to (7). The SAXS profile at the time shown by the arrow numbered (1) will be compared to the SAXS profile equilibrium at 220 °C in Figure 8a.

Figure 3 presents the time evolution of the peak intensity, $I_m = I(q=q_m)$, after *T*-drop to 175 °C (deep quench) and 182.5 °C (shallow quench). The values of I_m were obtained from the SAXS profiles corrected for the slit smearings. The arrows with the numbers in parentheses indicate the time when the TEM observations were done. The following features are found in Figure 3. The I_m stays a constant value for a certain incubation period after *T*-drop. After this period, the I_m at 175 and 182.5 °C starts to increase at about 500 and 4500 s, respectively.

(2) SAXS Profiles Measured before and after Freezing. The specimens were frozen with ice−water at a particular time during the orderings at the shallow quench to explore the transient ordered structures with TEM. The profiles were measured before and after freezing to check whether the freezing process changed

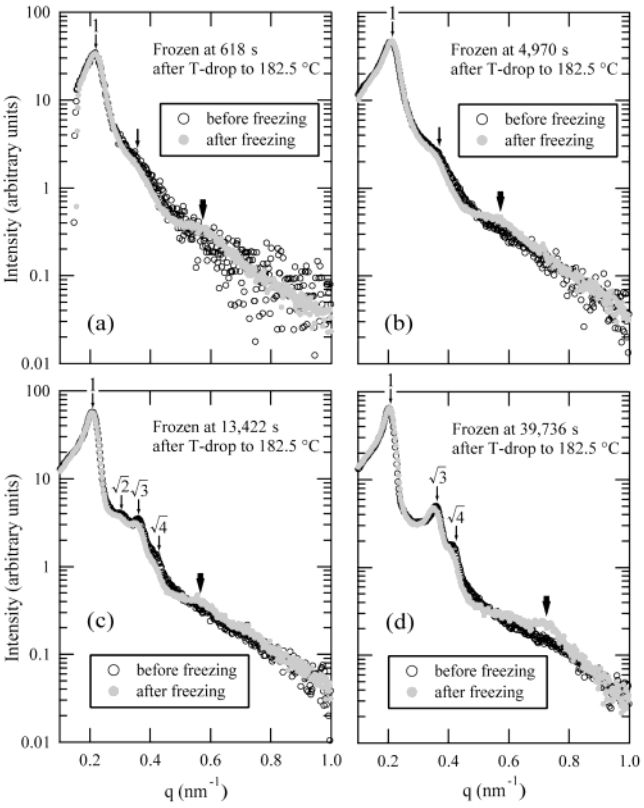

Figure 4. Comparison of the smeared SAXS profiles measured for the specimens before (open circles) and after (filled circles) freezing at (a) 618, (b) 4970, (c) 13 422, and (d) 39 736 s after *T*-drop to 182.5 °C.

the structure in the system. Figure 4 shows the SAXS profiles measured before and after freezing at (a) 618, (b) 4970, (c) 13 422, and (d) 39 736 s after *T*-drop to 182.5 °C (shallow quench), each of which corresponds to points (4)−(7) in Figure 3. Similar studies were carried out previously[65] for the deep quench at the times indicated by points (2) and (3) in Figure 3.

In parts a and b of Figure 4, both profiles after and before freezing have a first-order peak at $q = 0.21$ and 0.20 nm^{-1}, respectively, and a broad second-order shoulder at $q = 0.35$ nm^{-1}, marked by a thin arrow. In Figure 4c, both profiles after and before freezing have a first-order peak at $q = 0.20$ nm^{-1} and higher-order peaks at $q = \sqrt{2}q_m$, $\sqrt{3}q_m$, and $\sqrt{4}q_m$. Common to parts (a)−(c), a broad scattering maximum at $q = 0.55$ nm^{-1}, marked by a thick arrow, can be observed in the profile after freezing but not in that before freezing. In Figure 4d, both profiles after and before freezing have a first-order peak at $q = 0.19$ nm^{-1} and higher-order peaks at $q = \sqrt{3}q_m$ and $\sqrt{4}q_m$. A broad scattering maximum that is shifted from $q = 0.55$ nm^{-1} to $q = 0.70$ nm^{-1}, marked by a thick arrow, can be observed in the profile after freezing but not in that before freezing.

It is revealed from Figure 4 that the freeze-in process hardly changes the characteristics of the scattering profiles at small q ($q < 0.4$ nm^{-1}) and hence those of the structure at a large length scale associated with spatial arrangement of spheres or cylinders. However the processes affect the scattering profiles at a large q region ($q > 0.4$ nm^{-1}) and hence local structures of the system, as will be discussed in section IV.

III.2. Real-Space Observations. TEM and POM observations were conducted for the specimens frozen with ice−water at a particular time during the orderings (see Figure 3). Figure 5 gives the TEM images for the specimen frozen at (a) 740 s and (b) 14 504 s after *T*-drop to 175 °C (deep quench), corresponding to points (2) and (3) in Figure 3, respectively. The details of the TEM observations were described elsewhere.[65] The image given in Figure 5a shows the transient structure for the specimen frozen just after the ordering started. Ordered grains are observed in the matrix of the less ordered phase. The less ordered phase is mainly composed of disordered sphere, as will be clarified later in section IV-2, but disordered cylinders also can be seen in some parts of the less ordered phase, e.g., in the regions enclosed by white circles. The ordered grains are composed of hexagonally packed PS cylinders in the PI matrix. The shape of the ordered grains in which the cylindrical axis aligns perpendicular to the cross section of the specimen is almost isotropic, but that in which

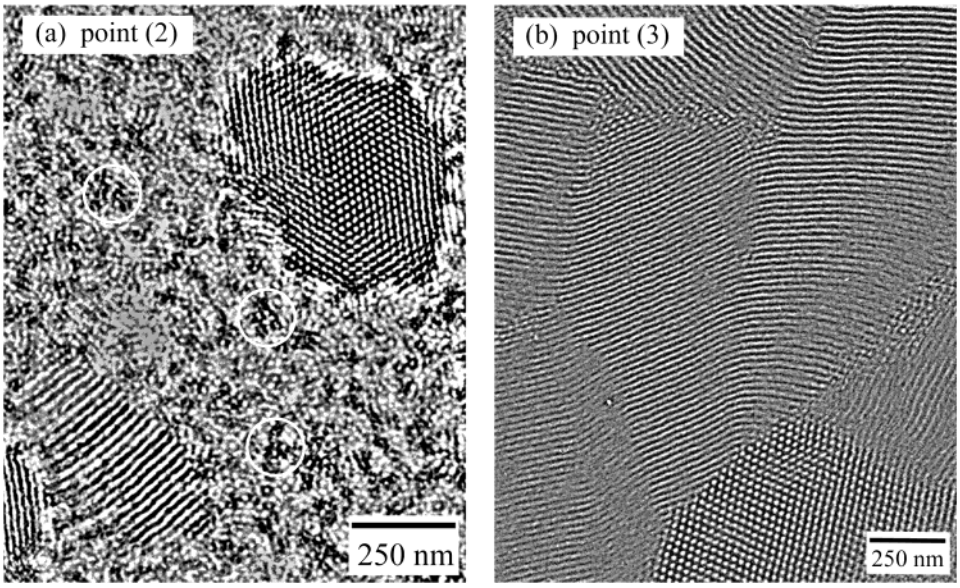

Figure 5. Transmission electron microscope images for the SIS triblock copolymer frozen at (a) 740 s (point (2) in Figure 3) and (b) 14 504 s (point (3) in Figure 3) after *T*-drop to 175 °C. The regions where distorted cylinders can be seen are encompassed by white circles.

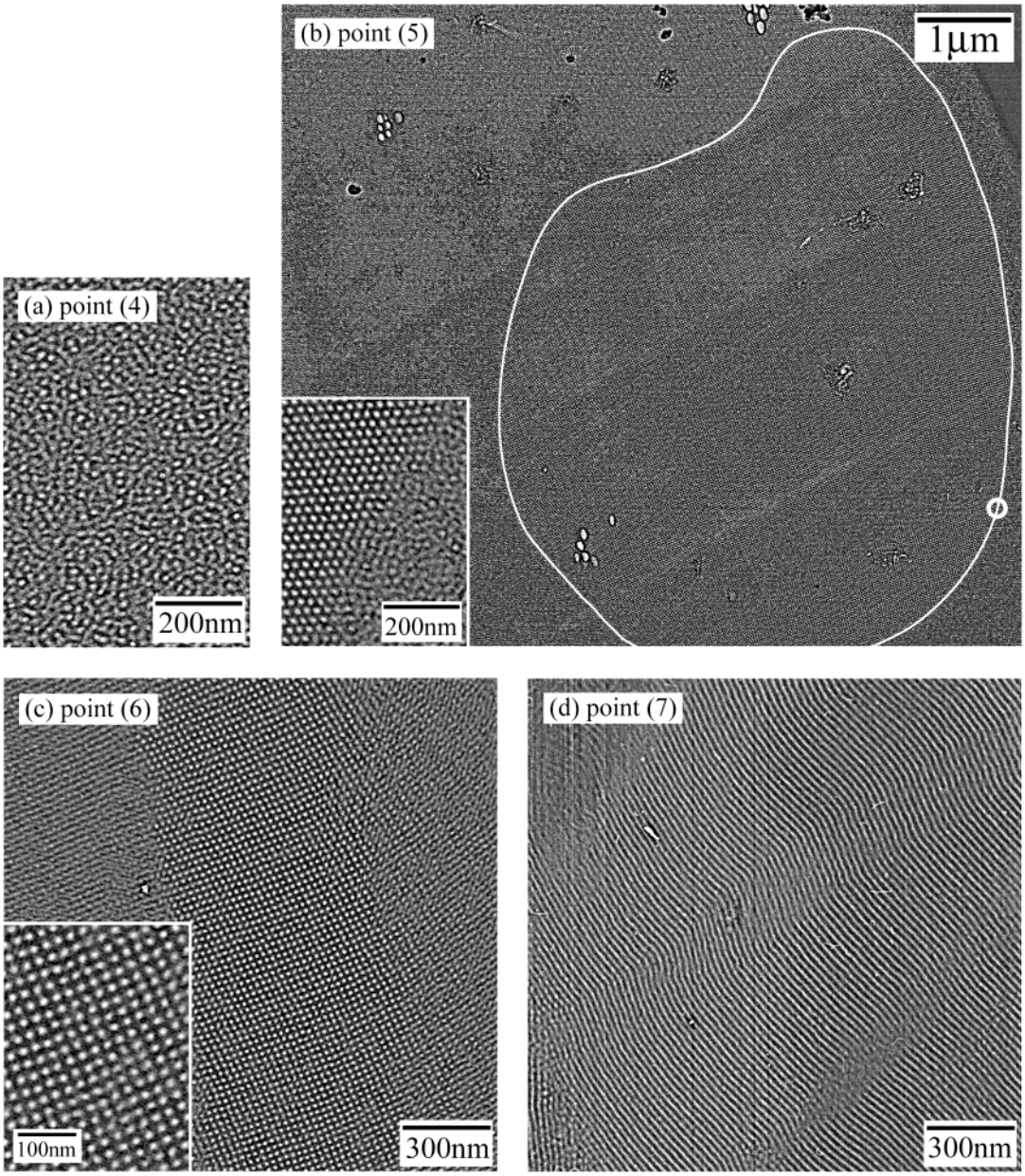

Figure 6. Transmission electron microscope images for the SIS triblock copolymer frozen at (a) 618, (b) 4970, (c) 13 422, and (d) 39 736 s (corresponding to points (4) to (7) in Figure 3, respectively) after *T*-drop to 182.5 °C. In (b), the white line traces the boundary between the ordered grain and the matrix phase. The inset enlarges the region encompassed by a small white circle and highlights the grain boundary, running nearly diagonally in the inset, between the ordered grain (left half) and the disordered-sphere phase (right half). In (c), the inset shows a magnified image of a center part of the low-magnification image.

the cylindrical axis aligns parallel to surfaces of the cross section of the specimen is anisotropic, revealing that the shape of the ordered grains in the matrix of disordered sphere is a lenslike oblate ellipsoid, where the cylinder axes are packed parallel to the short axis (the revolution axis) of the oblate ellipsoid. The details of the shape of the ordered grains should be referred to ref 65. The image given in Figure 5b shows the structure for the specimen frozen at the time when the ordering is almost completed. Many ordered grains fill whole the space. The ordered phase is covered with hexagonally packed PS cylinders in the PI matrix.

Figure 6 gives the TEM images for the specimen frozen at (a) 618, (b) 4970, (c) 13 422, and (d) 39 736 s after *T*-drop to 182.5 °C (shallow quench), corresponding to points (4)−(7) in Figure 3. Figure 7 represents the POM image for the specimen frozen at 39 736 s after *T*-drop to 182.5 °C (shallow quench). The POM images for the specimen frozen at (a) 618, (b) 4970, and (c) 13 422 s are not showed here, but the details of them will be described later.

The image given in Figure 6a shows the structure in the incubation period. The microdomain structure is very similar to that presented in Figure 1d in ref 16 and Figures 7 and 8 in ref 65, showing disordered sphere at 220 °C (above T_{LDOT}). The microdomain structure appears to be composed of small bright PS spheres with diameter $\sim$ 25 nm and dark PI matrix. The PS spheres are arranged in space with only a short-range liquidlike order. Random displacement of centers of spheres and overlapping of them in ultrathin sections along the incident electron beam axis tend to give us an impression as if they were interconnected. The overlaps tend to give a contrast variation for the PS domains in the image. It may be also possible that some of PS domains are interconnected.

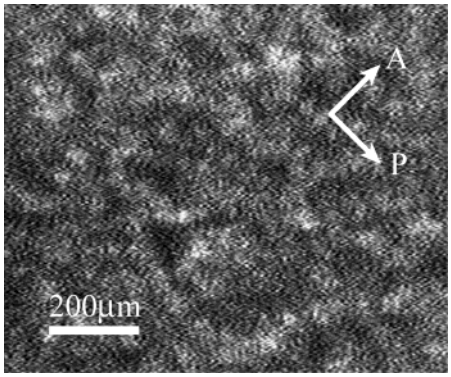

Figure 7. POM image under crossed polarizers for the SIS triblock copolymer frozen at 39 736 s (point (7) in Figure 3) after *T*-drop to 182.5 °C.

The TEM image given in Figure 6b shows a transient structure for the specimen frozen just after the ordering started. An ordered grain is observed in the matrix of the less ordered phase. The periphery of the ordered grain is traced by a white line to clarify the grain boundary between the ordered phase and the less ordered phase in the low-magnification image. It is found that the shape of the ordered grain is almost isotropic, and its size is more than 7 μm in diameter. The inset highlights the boundary between the ordered grain and the less ordered phase, at the position enclosed by a bright circle. The bright PS round domains on the left-hand side in the inset regularly align with hexagonal symmetry, while the PS domains on the right side align randomly. The less ordered matrix is similar to the structure observed in Figure 6a. The POM observation conducted for this specimen showed the image uniformly dark and featureless, though the result is not shown here. This result suggests that the shape of the microdomains is spherical as will be discussed later in section IV.

The TEM image in Figure 6c shows a transient structure during the ordering process at point (6) in Figure 3. The round microdomains with a long-range order fill the whole sample space. The inset highlights the microdomain structure. The round microdomains are packed in a square lattice. The POM observation was also conducted for this specimen. However, the image was uniformly dark and featureless. This result also suggests that the shape of the microdomains is spherical.

The TEM image given in Figure 6d is a structure for the specimen frozen at the time when the ordering is almost completed at point (7) in Figure 3. The ordered phase fills the whole space. The TEM image is composed of the alternative dark and bright stripes, which corresponds to the ultrathin section cut parallel to the cylinder axis. The POM observation was also conducted for this specimen. The POM image can be seen due to the form birefringence,[75] as shown in Figure 7. The image is composed of dark and bright grains with an average grain size of 60 μm in diameter, reflecting that the grains composed of hex-cylinder with their "directors" (average orientation of cylinder axes in the grains) changing from a grain to a grain.

IV. Discussion

IV.1. Ordering of Hex-Cylinder Induced by Deep Quench. The ordering process into hex-cylinder induced by a deep quench has already been reported.[65] However, we will summarize it briefly in order to facilitate comparisons of the ordering process induced by a shallow quench.

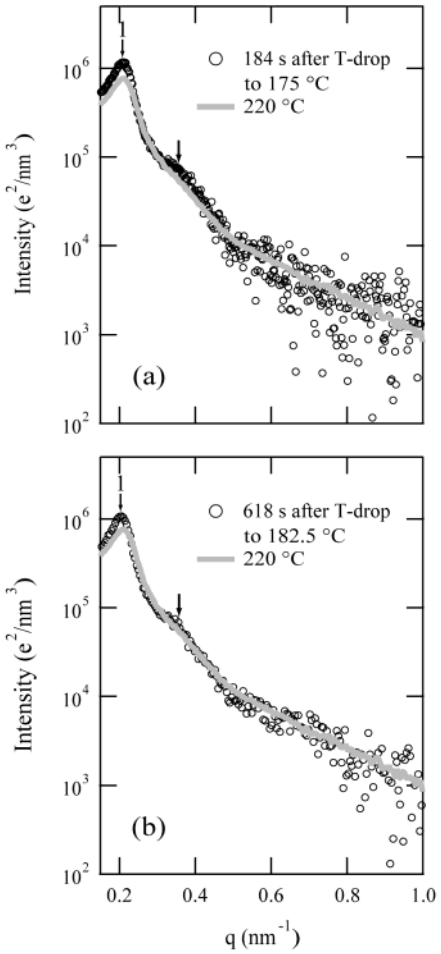

Figure 8. Comparison of the measured SAXS profiles in equilibrium at 220 °C above T_{LDOT} (solid line) with transient SAXS profiles measured (a) at 184 s (point (1) in Figure 3) after *T*-drop to 175 °C and (b) at 618 s (point (4) in Figure 3) after *T*-drop to 182.5 °C (○).

The ordering induced by the deep quench proceeds as follows. The system stays at a disordered-sphere state for a certain incubation period as long as about 500 s as evidenced by the time-independent I_m in Figure 3. This is also evidenced by the broad second-order shoulder in the SAXS profile at 184 s after *T*-drop (see Figure 2a) and the TEM observation (see Figure 8 in ref 65). In Figure 8a, the SAXS profile at 184 s after *T*-drop to 175 °C (corresponding to point (1) in Figure 3) is shown to compare with that measured at 220 °C above T_{LDOT} in a static SAXS experiment,[16,65] where disordered sphere is an equilibrium state. The two SAXS profiles are essentially identical, though there are some subtle differences as will be clarified below. Thus, it is clearly concluded that disordered sphere exists as a metastable structure in the incubation period. The first-order peak of the former SAXS profile is sharper than that of the latter one, and the second-order shoulder, marked by a thin arrow, of the former one is more distinct than that of the latter one. These indicate that centers of spheres in the supercooled disordered-sphere state at 175 °C in the incubation period are less randomly distributed than those in the equilibrium disordered-sphere state at 220 °C. Thus, in our system we do not find spinodal decomposition process for the transformation from

disordered sphere to hex-cylinder. The spinodal decomposition mechanism, however, might come into play in the transformation process at deeper quenches from T_{OOT}.

After the incubation period, the I_m starts to increase at ~500 s, as illuminated by the higher-order peaks at $q = \sqrt{3}q_m$ and $\sqrt{4}q_m$ in the SAXS profiles (Figure 2a). These indicate that the ordering of hex-cylinder started. In Figure 5, the TEM image (a) for the specimen just after the ordering started shows the coexistence of the ordered grains composed of hex-cylinder and disordered sphere. The existence of the incubation period together with the coexistence suggests that the ordering proceeds via the nucleation and growth process. The TEM image (b) for the specimen frozen at the time when the ordering is almost completed shows the volume-filling grains of hex-cylinder. The results shown in Figure 5 illuminate that the ordered grains grow at the expense of disordered sphere. Therefore, it is concluded that hex-cylinder is directly transformed from disordered sphere via the nucleation and growth process in the ordering process induced by the deep quench below the T_{OOT}.

IV.2. Ordering of Hex-Cylinder Induced by Shallow Quench. Now we will discuss the ordering process induced by a shallow quench into hex-cylinder. In Figure 3, the time evolution of the I_m after *T*-drop to 182.5 °C shows a similar trend to that after *T*-drop to 175 °C. The I_m stays at a disordered-sphere state for a certain incubation period, after which the I_m starts to increase at 4500 s, indicating that the ordering starts. The existence of the incubation period suggests that this ordering also proceeds via the nucleation and growth process.

The SAXS profile at 618 s after *T*-drop to 182.5 °C in Figure 2b and that in Figure 4a show a broad second-order shoulder which is the same as that in the SAXS profile at 184 s after *T*-drop to 175 °C. Besides, the scattering maximum marked by a thick arrow appears in the SAXS profile after freezing as shown in Figure 4a. This corresponds to the maximum of the particle scattering from the spheres, i.e., the maximum from the form factor, which is believed to appear because the interface between PS spheres and PI matrix is sharpened by lowering temperature. The microdomain structure in Figure 6a is similar to that in Figure 8 of ref 65 and that in Figure 1d of ref 16. These pieces of evidence indicate that the system is in the supercooled disordered-sphere phase in the incubation period. In Figure 8b, the SAXS profile at 618 s (corresponding to point (4) in Figure 3) after *T*-drop to 182.5 °C is shown to compare with that measured in situ at 220 °C in the static SAXS experiment.[16,65] The same features as Figure 8a can be seen. Therefore, centers of spheres in the supercooled disordered-sphere state at 182.5 °C in the incubation period are also less randomly distributed than those in the equilibrium disordered-sphere state at 220 °C.

In Figure 2b, higher-order peaks start to appear as the ordering proceeds. Moreover, the higher-order peaks can be seen at $q = \sqrt{2}q_m$, $\sqrt{3}q_m$, and $\sqrt{4}q_m$ in the SAXS profile at 13 312 s. As time further elapses, the higher-order peak at $q = \sqrt{2}q_m$ disappears, and those at $q = \sqrt{3}q_m$ and $\sqrt{4}q_m$ are getting sharper. Therefore, it is revealed that the time evolution of the SAXS profiles at the shallow quench is clearly different from that at the deep quench, implying a different pathway according to which disordered sphere is transformed into an equilibrium hex-cylinder.

Let us discuss the results on the real-space observations in order to understand the ordering process induced by this shallow quench in detail. Figure 6b shows the TEM image for the specimen frozen just after the ordering started (point (5) in Figure 3). The coexistence of the ordered grain existing inside the region encompassed by the white line and the less ordered phase (outside the region) are observed in this image. The less ordered phase is similar to the structure in Figure 6a (see the right half of the image shown in the inset of Figure 6b), indicating that it is composed of disordered sphere. The bright round domains aligned with hexagonal symmetry and with long-range order can be seen in the ordered grain (see the left half of the inset). The higher-order SAXS peak cannot be seen clearly as shown in Figures 2b and 4b. It reflects that the volume fraction of the ordered grains is still not large enough to exhibit the diffraction peaks. The POM image was uniformly dark and featureless; that is to say, the form birefringence due to ordered microdomains did not exist in this system. These indicate that the round shape of the microdomain structure in the ordered grains is spherical. Therefore, the image in the ordered grains shown in the inset is best interpreted as an image viewed along the [111] direction of bcc-sphere. The coexistence of the ordered grain and the disordered spheres also supports that this ordering proceeds by the nucleation and growth process. This is a surprise at a first glance because the ordering below T_{OOT} does not nucleate cylindrical domain structures.

Figure 6c shows the TEM image for the specimen frozen at the time when the ordering is going on (point (6) in Figure 3). From this TEM image together with the SAXS profile at 13 312 s shown in Figure 2b, we expect the ordered grains composed of the volume-filled spherical microdomains. This expectation is supported by the following two pieces of evidence: The higher-order peaks can be seen at $q = \sqrt{2}q_m$, $\sqrt{3}q_m$, and $\sqrt{4}q_m$ in the SAXS profiles of Figure 4c, and the maximum of the particle scattering from the spheres can be seen at $q = 0.55$ nm^{-1} in the SAXS profile after freezing (marked by a thick arrow). The POM image was uniformly dark and featureless. All these results together indicate that bcc-sphere fills whole the space at this time after *T*-drop, and its (100) plane is seen in the inset of this TEM image. Note that some parts of the low-magnification image in Figure 6c are not clear, which is believed to be due to overlap of bcc-sphere along the thickness direction of the ultrathin section, and electron beams propagate along off-symmetry axes.

Figure 6d and Figure 7 show the TEM image and the POM image for the specimen frozen at the time when the ordering is almost completed (point (7) in Figure 3). It is observed in Figure 6d that the ordered phase fills the whole space. The higher-order SAXS peaks can be seen only at $q = \sqrt{3}q_m$ and $\sqrt{4}q_m$ in Figures 2b and 4d, and the image due to the form birefringence can be seen in the POM image of Figure 7. Therefore, the morphology of this ordered phase is concluded to be hex-cylinder. Moreover, the SAXS profile after freezing shown in Figure 4d revealed an obvious shift of the form factor scattering maximum (marked by a thick arrow) from $q = 0.55$ nm^{-1} (in part c) to $q = 0.72$ nm^{-1} (in part d). The scattering maximum corresponds to cylinders rather than spheres. The average radius of the cylinders and the spheres evaluated from the form factor peak in parts d and c are 7.1 and 10.5 nm, respectively.[76] These

values together with the q_m values yielded the volume fraction of the cylinders and the spheres as evaluated by SAXS[76] to be 0.13 and 0.11, respectively, which are consistent with the stoichiometric volume fraction calculated from the composition of the block copolymer, 0.16. This evidence also supports that hex-cylinder is formed at this time in the system.

Consequently, we can conclude that the ordering process induced by the shallow quench below T_{OOT} into hex-cylinder proceeds as follows. First, spherical microdomains order into a bcc lattice via the nucleation and growth process after a certain incubation period. The ordered grains of bcc-sphere grow at the expense of disordered sphere, and then bcc-sphere fills the whole sample space, despite the fact that the system exists below T_{OOT} where hex-cylinder is an equilibrium morphology. Subsequently, bcc-sphere is transformed into hex-cylinder. Finally, hex-cylinder fills the whole space. It is revealed that the ordering process of hex-cylinder induced by the shallow quench involves first the formation of a metastable bcc-sphere followed by the OOT from bcc-sphere to hex-cylinder. Whether the OOT from bcc-sphere to hex-cylinder occurs via nucleation and growth[34,37] or spinodal decomposition[36] is beyond the scope of this work and deserve future work.

IV.3. Comments on Kinetic Pathways of the Ordering in the SIS Triblock Copolymer. As described above, we discovered a profound difference in the ordering processes from disordered sphere to hex-cylinder at the small and large quench depths with respect to T_{OOT}, ΔT. The experimental results would lead us to visualize possible kinetic pathways for these two cases. Figure 9 represents the pathways at a shallow quench, ΔT_1, and a deep quench, ΔT_2, for block copolymers with a given block composition. It should be noted that the pathway depends on the composition. At the deep quench, ΔT_2, the system transforms directly from disordered sphere with free energy, G_d, to hex-cylinder with free energy, G_2 ($<G_d$), via a free energy barrier, ΔG_2, for the observed nucleation process. On the other hand, at the shallow quench, ΔT_1, the system transforms into hex-cylinder with free energy, G_1 ($>G_2$), through the metastable bcc-sphere with free energy G_{1m} ($G_1 < G_{1m} < G_d$). The transformation from disordered sphere to the metastable bcc-sphere involves a free energy barrier, ΔG_{11}, and the transformation from the metastable bcc-sphere to hex-cylinder would also involve a free energy barrier, ΔG_{12}. ΔG_{11} should be much larger than ΔG_2, judging from the much longer incubation time for the quench with ΔT_1 than for that with ΔT_2. ΔG_{12} is expected to exist because the transformation into hex-cylinder occurs only after the formation of the volume-filling bcc-sphere phase.

Now we would like to note the reason why nature selects the two-step phase transformation rather than a single-step transformation at the shallow quench. The single-step transformation involves cooperative transformation of the structural units from spheres to cylinders and transient coexistence of the hex-cylinder phase with the disordered-sphere phase, as schematically shown in Figure 10a. The free energy barrier, ΔG_1, involved in this process is expected to be larger than ΔG_{11} for the system having the transient coexistence of the bcc-sphere phase and the disordered-sphere phase, as schematically shown in Figure 10b. A crude speculation for this expectation is given as follows. The conformational entropy loss associated with packing of PI

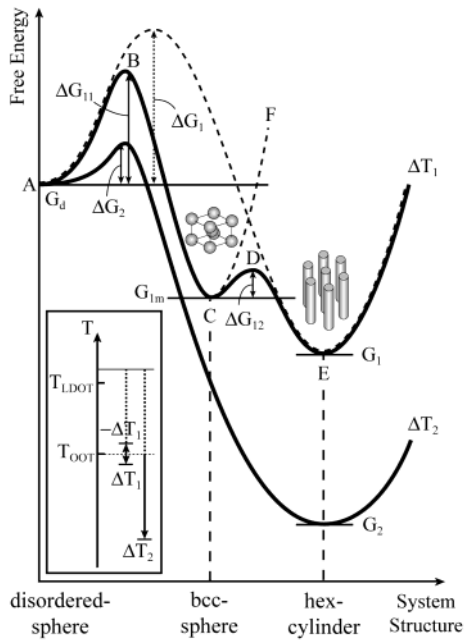

Figure 9. Schematic diagrams showing possible kinetic pathways after T-drop for the phase transformation of the system with the two quench depths from the OOT. The solid lines show pathways at ΔT_1 (shallow quench) and ΔT_2 (deep quench), and the broken line shows a kinetic pathway expected for a direct transformation from disordered sphere to hex-cylinder at ΔT_1. The pathway shown by A → B → C → F is the one expected for the transformation from disordered sphere to bcc-sphere at the quench depth of $-\Delta T_1$ as indicated in the inset. ΔG_1 and ΔG_{11} represent the heights of the energy barriers for nucleation of hex-cylinder and the metastable bcc-sphere from disordered sphere, respectively. ΔG_{12} represents the height of the energy barrier for nucleation of hex-cylinder in the matrix of the metastable bcc-sphere.

blocks in the SIS, at the boundary between the ordered phase of hex-cylinder or bcc-sphere and the disordered phase of disordered sphere (as schematically illustrated in the inset of part a or b), will make a significant contribution to the interfacial free energy between the ordered phase and the mother phase (disordered sphere). The ordered phase of hex-cylinder is expected to have a higher interface free energy than the ordered phase of bcc-sphere, simply because the former phase is expected to encounter a large conformational entropy loss at the interface with the mother phase than the latter phase. Moreover, the bulk free energies of bcc-sphere and hex-cylinder are expected to be not much different at a small ΔT limit in the hex-cylinder phase. Those two factors described above may explain $\Delta G_1 > \Delta G_{11}$, thus favoring the two-step transformation rather than the single-step transformation. The metastable bcc-sphere is then transformed into hex-cylinder via deformation of spheres and interconnection of deformed spheres along the [111] direction of bcc-sphere as clarified by previous reports.[32,35,36]

As will be reported in a companion paper,[78] the incubation time for the metastable bcc-sphere at T_{cyl} exists on a point along the extrapolation line of incubation time vs quench depth for bcc-sphere, ΔT_{sph} ($\equiv T_{LDOT} - T_{sph}$) with T_{sph} ($T_{OOT} \le T_{sph} \le T_{LDOT}$) being the temperature where disordered sphere is transformed into the equilibrium bcc-sphere. For the shallow quench of ΔT_1, the incubation time is nearly equal to that at $-\Delta T_1$ ($\equiv T_{OOT} - T_{sph}$), as defined in the inset of Figure 9, where an equilibrium bcc-sphere is formed.

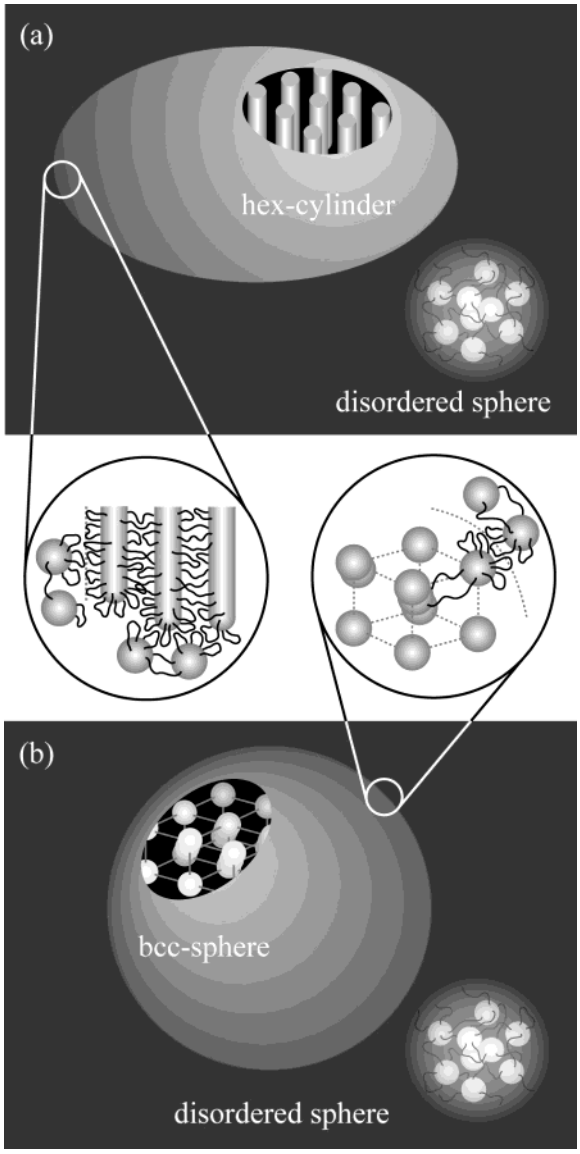

Figure 10. Schematic illustrations of the coexistence of (a) the ordered phase composed of hex-cylinder (grey phase) and the phase composed of disordered sphere (dark phase) and (b) the phase composed of bcc-sphere (grey phase) and the phase composed of disordered sphere (dark phase). The spatial arrangement of spheres with short-range liquidlike order, which is only partly indicated schematically in the bottom right corner in the disordered-sphere phase, extends whole the dark disordered phase. The insets to (a) and (b) respectively represent local packing interactions of PI block chains emanating from the disordered spheres and those emanating from hex-cylinder and bcc-sphere.

Therefore, ΔG_{11} is expected to be close to the free energy barrier for the nucleation process of bcc-sphere at $-\Delta T_1$, i.e., $\Delta G(-\Delta T_1)$. Moreover, G_{1m} is also expected to be close to the free energy of the equilibrium bcc-sphere at $-\Delta T_1$, i.e., $G(-\Delta T_1)$. Thus, the kinetic pathway of A → B → C at ΔT_1 may be close to that at $-\Delta T_1$. A clear difference is seen in the pathway from C to F at $-\Delta T_1$ and from C to D to E at ΔT_1.

Finally, we would like to comment on the kinetic pathways of ODTs reported by Qi and Wang.[79] They studied the kinetic pathways of hex-cylinder to disordered state after a sudden temperature-jump (T-jump) by using the computer simulation based on the time-dependent Ginzburg−Landau equation. Their analysis ignores thermal fluctuation effects[2,80,81] on the phase transition which should be quite important for any systems having structures with a small periodicity. For a large T-jump deep into the disordered state, they find that hex-cylinder melts uniformly; i.e., hex-cylinder is directly transformed into the disordered state. However, when a small T-jump only slightly into the disordered state is imposed to the system, the melting of hex-cylinder goes through a transient bcc-sphere; i.e., bcc-sphere is once formed as an intermediate state during the phase transition from hex-cylinder to the disordered state. The phase transition process in their study is just opposite to that in our study, but the processes are superficially similar. It would be interesting to conduct computer simulations for the phase transition form a disordered state to hex-cylinder as a function of ΔT and to conduct T-jump experiments from a hex-cylinder to a disordered-sphere phase as a function of superheating, ΔT_{dis} ($\equiv T - T_{LDOT}$).

V. Concluding Remarks

In this work, we presented the ordering processes induced by the phase transition from disordered sphere to hex-cylinder for the SIS triblock copolymer by using time-resolved SAXS, combined with TEM and POM observations. As reported earlier,[65] the transformation process induced by a deep quench into hex-cylinder is confirmed to proceed as follows: After T-drop, the system stays in the supercooled disordered-sphere phase for a certain incubation period. After this incubation period, the grains composed of hex-cylinder are nucleated in the disordered-sphere phase and grow at the expense of the disordered-sphere phase; i.e., hex-cylinder is directly transformed from the disordered sphere. On the other hand, the transformation process induced by a shallow quench into hex-cylinder proceeds as follows: The system stays in the supercooled disordered-sphere phase for a certain incubation period in this case, too. After this incubation period, the grains composed of bcc-sphere appear in the disordered-sphere phase and grow at the expense of the disordered-sphere phase. After bcc-sphere fills the whole sample space, bcc-sphere is transformed into hex-cylinder. In this process, the system first forms the volume-filling metastable bcc-sphere, followed by OOT into hex-cylinder. A conjecture for the two-step phase transformation is presented in section IV.3 of the text.

Acknowledgment. The authors gratefully acknowledge Prof. C. D. Han for providing the interesting block copolymer sample. T.H. gratefully acknowledges financial support by a Grant-in-Aid for Scientific Research (under Grant 12305060(A)) from Japan Society for the Promotion of Science and by 21st Century COE Program for an United Approach to New Materials Science.

References and Notes

(1) Leibler, L. *Macromolecules* **1980**, *13*, 1602−1617.
(2) Fredrickson, G. H.; Helfand, E. *J. Chem. Phys.* **1987**, *87*, 697−705.
(3) See, for example: Hashimoto, T. In *Thermoplastic Elastomers*, 1st ed.; Legge, N. R., Holden, G. R., Schroeder, H. E., Eds.; Hanser: Vienna, 1987; Chapter 12, Section 3, p 349, and 2nd ed.; 1996; Chapter 15A, p 429, and references therein.
(4) See for example: Bates, F. S.; Fredrickson, G. H. *Annu. Rev. Phys. Chem.* **1990**, *41*, 525. Bates, F. S.; Fredrickson, G. H. In *Thermoplastic Elastomers*, 2nd ed.; Legge, N. R., Holden, G. R., Schroeder, H. E., Eds.; Hanser: Vienna, 1996; Chapter 12, p 335, and references therein.

(5) Bates, F. S.; Rosedale, J. H.; Fredrickson, G. H. *J. Chem. Phys.* **1990**, *92*, 6255−6270.
(6) Stühn, B.; Mutter, R.; Albrecht, T. *Europhys. Lett.* **1992**, *18*, 427−432.
(7) Wolff, T.; Burger, C.; Ruland, W. *Macromolecules* **1993**, *26*, 1707−1711.
(8) Hashimoto, T.; Ogawa, T.; Han, C. D. *J. Phys. Soc. Jpn.* **1994**, *63*, 2206−2214.
(9) Sakamoto, N.; Hashimoto, T. *Macromolecules* **1995**, *28*, 6825−6834.
(10) Han, C. D.; Baek, D. M.; Kim, J. K.; Ogawa, T.; Sakamoto, N.; Hashimoto, T. *Macromolecules* **1995**, *28*, 5043−5062.
(11) Ogawa, T.; Sakamoto, N.; Hashimoto, T.; Han, C. D.; Baek, D. M. *Macromolecules* **1996**, *29*, 2113−2123.
(12) Hashimoto, T.; Shibayama, M.; Kawai, H.; Watanabe, H.; Kotaka, T. *Macromolecules* **1983**, *16*, 361−371.
(13) Schwab, M.; Stühn, B. *Phys. Rev. Lett.* **1996**, *76*, 924−927.
(14) Schwab, M.; Stühn, B. *Colloid Polym. Sci.* **1997**, *275*, 341−351.
(15) Sakamoto, N.; Hashimoto, T.; Han, C. D.; Kim, D.; Vaidya, N. Y. *Macromolecules* **1997**, *30*, 1621−1632.
(16) Sakamoto, N.; Hashimoto, T.; Han, C. D.; Kim, D.; Vaidya, N. Y. *Macromolecules* **1997**, *30*, 5321−5330.
(17) Han, C. D.; Vaidya, N. Y.; Kim, D.; Shin, G.; Yamaguchi, D.; Hashimoto, T. *Macromolecules* **2000**, *33*, 3767−3780.
(18) Vaidya, N. Y.; Han, C. D.; Kim, D.; Sakamoto, N.; Hashimoto, T. *Macromolecules* **2001**, *34*, 222−234.
(19) Choi, S.; Lee, K. M.; Han, C. D.; Sota, N.; Hashimoto, T. *Macromolecules* **2003**, *36*, 793−803.
(20) Helfand, E.; Wasserman, Z. R. In *Developments in Block Copolymers*; Goodman, I., Ed.; Applied Science: London, 1982; Vol. 1, Chapter 4, p 99.
(21) Hashimoto, T.; Shibayama, M.; Fujimura, M.; Kawai, H. In *Block Copolymers, Science and Technology*; Meier, D. J., Ed.; Harwood Academic Publishers: London, 1983; p 63.
(22) Hasegawa, H.; Tanaka, H.; Yamasaki, K.; Hashimoto, T. *Macromolecules* **1987**, *20*, 1651−1662.
(23) Vavasour, J. D.; Whitmore, M. D. *Macromolecules* **1992**, *25*, 5477−5486.
(24) Matsen, M. W.; Bates, F. S. *Macromolecules* **1996**, *29*, 1091−1098.
(25) Laradji, M.; Shi, A.-C.; Noolandi, J.; Desai, R. C. *Macromolecules* **1997**, *30*, 3242−3255.
(26) Förster, S.; Khandpur, A. K.; Zhao, J.; Bates, F. S.; Hamley, I. W.; Ryan, A. J.; Bras, W. *Macromolecules* **1994**, *27*, 6922−6935.
(27) Khandpur, A. K.; Förster, S.; Bates, F. S.; Hamley, I. W.; Ryan, A. J.; Bras, W.; Almdal, K.; Mortensen, K. *Macromolecules* **1995**, *28*, 8796−8806.
(28) Sakurai, S.; Momii, T.; Taie, K.; Shibayama, M.; Nomura, S. *Macromolecules* **1993**, *26*, 485−491.
(29) Sakurai, S.; Umeda, H.; Taie, K.; Nomura, S. *J. Chem. Phys.* **1996**, *105*, 8902−8908.
(30) Hajduk, D. A.; Gruner, S. M.; Rangarajan, P.; Register, R. A.; Fetters, L. J.; Honeker, C.; Albalak, R. J.; Thomas, E. L. *Macromolecules* **1994**, *27*, 490−501.
(31) Sakurai, S.; Kawada, H.; Hashimoto, T.; Fetters, L. J. *Macromolecules* **1993**, *26*, 5796−5802.
(32) Sakurai, S.; Hashimoto, T.; Fetters, L. J. *Macromolecules* **1996**, *29*, 740−747.
(33) Ryu, C. Y.; Lee, M. S.; Hajduk, D. A.; Lodge, T. P. *J. Polym. Sci., Polym. Phys. Ed.* **1997**, *35*, 2811−2823.
(34) Ryu C. Y.; Lodge, T. P. *Macromolecules* **1999**, *32*, 7190−7201.
(35) Kimishima, K.; Koga, T.; Hashimoto, T. *Macromolecules* **2000**, *33*, 968−977.
(36) Kimishima, K.; Koga, T.; Kanazawa, Y.; Hashimoto, T. *ACS Symp. Ser.* **2000**, *739*, Chapter 32, 514−530.
(37) Lee, H. H.; Jeong, W.-Y.; Kim, J. K.; Ihn, K. J.; Kornfield, J. A.; Wang, Z.-G.; Qi, S. *Macromolecules* **2002**, *35*, 785−794.
(38) Hajduk, D. A.; Takenouchi, H.; Hillmyer, M. A.; Bates, F. S.; Vigild, M. E.; Almdal, K. *Macromolecules* **1997**, *30*, 3788−3795.
(39) Hajduk, D. A.; Ho, R. M.; Hillmyer, M. A.; Bates, F. S.; Almdal, K. *J. Phys. Chem. B* **1998**, *102*, 1356−1363.
(40) Sakurai, S.; Umeda, H.; Furukawa, C.; Irie, H.; Nomura, S.; Lee, H. H.; Kim, J. K. *J. Chem. Phys.* **1998**, *108*, 4333−4339.
(41) Hamley, I. W.; Fairclough, J. P. A.; Ryan, A. J.; Mai, S.-M.; Booth, C. *Phys. Chem. Chem. Phys.* **1999**, *1*, 2097−2101.
(42) Schulz, M. F.; Bates, F. S.; Almdal, K.; Mortensen, K. *Phys. Rev. Lett.* **1994**, *73*, 86−89.
(43) Vigild, M. E.; Almdal, K.; Mortensen, K.; Hamley, I. W.; Fairclough, J. P. A.; Ryan, A. J. *Macromolecules* **1998**, *31*, 5702−5716.
(44) Floudas, G.; Ulrich, R.; Wiesner, U. *J. Chem. Phys.* **1999**, *110*, 652−663.
(45) Wang, C.-Y.; Lodge, T. P. *Macromolecules* **2002**, *35*, 6997−7006.
(46) Floudas, G.; Ulrich, R.; Wiesner, U.; Chu, B *Europhys. Lett.* **2000**, *50*, 182−188.
(47) Hashimoto, T. *Macromolecules* **1987**, *20*, 465−468.
(48) Harkless, C. R.; Singh, M. A.; Nagler, S. E.; Stephenson, G. B.; Jordan-Sweet, J. L. *Phys. Rev. Lett.* **1990**, *64*, 2285−2288.
(49) Singh, M. A.; Harkless, C. R.; Nagler, S. E.; Shannon, Jr., R. F.; Ghosh, S. S. *Phys. Rev. B* **1993**, *47*, 8425−8435.
(50) Schuler, M.; Stühn, B. *Macromolecules* **1993**, *26*, 112−113.
(51) Stühn, B.; Vilesov, A.; Zachmann, H. G. *Macromolecules* **1994**, *27*, 3560−3565.
(52) Hashimoto, T.; Sakamoto, N. *Macromolecules* **1995**, *28*, 4779−4781.
(53) Adams, J. L.; Quiram, D. J.; Graessley, W. W.; Register, R. A.; Marchand, G. R. *Macromolecules* **1996**, *29*, 2929−2938.
(54) Hashimoto, T.; Sakamoto, N.; Koga, T. *Phys. Rev. E* **1996**, *54*, 5832−5835.
(55) Hashimoto, T.; Ogawa, T.; Sakamoto, N.; Ichimiya, M.; Kim, J. K.; Han, C. D. *Polymer* **1998**, *39*, 1573−1581.
(56) Hajduck, D. A.; Tepe, T.; Takenouchi, H.; Tirrell, M.; Bates, F. S. *J. Chem. Phys.* **1998**, *108*, 326−333.
(57) Rosedale, J. H.; Bates, F. S. *Macromolecules* **1990**, *23*, 2329−2338.
(58) Floudas, G.; Pakula, T.; Fischer, E. W.; Hadichristidis, N.; Pispas, S. *Acta Polym.* **1994**, *45*, 176−181.
(59) Floudas, G.; Hadichristidis, N.; Iatrou, H.; Pakula, T.; Fischer, E. W. *Macromolecules* **1994**, *28*, 7735−7746.
(60) Floudas, G.; Fytas, G.; Hadichristidis, N.; Pitsikalis, M. *Macromolecules* **1995**, *28*, 2359−2362.
(61) Newstein, M. C.; Garetz, B. A.; Dai, H. J.; Balsara, N. P. *Macromolecules* **1995**, *28*, 4587−4597.
(62) Dai, H. J.; Balsara, B. A.; Garetz, B. A.; Newstein, M. C. *Phys. Rev. Lett.* **1996**, *77*, 3677−3680.
(63) Sakamoto, N.; Hashimoto, T. *Macromolecules* **1998**, *31*, 3292−3302.
(64) Sakamoto, N.; Hashimoto, T. *Macromolecules* **1998**, *31*, 3815−3823.
(65) Sakamoto, N.; Hashimoto, T. *Macromolecules* **1998**, *31*, 8493−8502.
(66) Fujimura, M.; Hashimoto, H.; Kurahashi, K.; Hashimoto, T.; Kawai, H. *Macromolecules* **1981**, *14*, 1196−1202.
(67) Fujimura, M.; Hashimoto, T.; Kawai,.H. *Mem. Fac. Eng., Kyoto Univ.* **1981**, *43* (2), 224.
(68) Hashimoto, T.; Suehiro, S.; Shibayama, M.; Saijo, K.; Kawai, H. *Polym. J.* **1981**, *13*, 501−516.
(69) Suehiro, S.; Saijo, K.; Ohta, Y.; Hashimoto, T.; Kawai, H. *Anal. Chim. Acta* **1986**, *189*, 41−56.
(70) Kortleve, G.; Tuynman, C. A. F.; Vonk, C. G. *J. Polym. Sci., Part A-2: Polym. Phys.* **1972**, *10*, 123−131.
(71) Hendricks, R. W. *J. Appl. Crystallogr.* **1972**, *5*, 315−324.
(72) Medellin-Rodriguez, F. J.; Philips, P. J.; Lin, J. S. *Macromolecules* **1996**, *29*, 7491−7501.
(73) Kato, K. *J. Polym. Sci., Part B: Polym. Lett.* **1966**, *4*, 35−38.
(74) Ribbe, A. E.; Bodycomb, J.; Hashimoto, T. *Macromolecules* **1999**, *32*, 3154−3156.
(75) Wiener, O. *Abh. Math.-Phys., Kl. Saechs. Ges. Wiss.* **1912**, *32*, 507.
(76) Shibayama, M.; Hashimoto, T.; Kawai, H. *Macromolecules* **1983**, *16*, 16−28.
(77) Ryu C. Y.; Lodge, T. P. *Macromolecules* **1999**, *32*, 7190−7201.
(78) Sota, N.; Sakamoto, N.; Hashimoto, T. Manuscript in preparation.
(79) Qi, S.; Wang, Z. G. *Phys. Rev. Lett.* **1996**, *76*, 1679−1682.
(80) Brazovskii, A. *Sov. Phys. JETP* **1975**, *41*, 85−90.
(81) Hashimoto, T.; Koga, T.; Koga, T.; Sakamoto, N. In *The Physics of Complex Liquids*; Yonezawa, F., Tsuji, K., Kaji, K., Doi, M., Fujiwara, T., Eds.; World Scientific: Singapore, 1998; p 291.

MA034291I